Supporting Information

Identification and Detection of Volatile Aldehydes as Lung Cancer Biomarkers by Vapor Generation Combined with Paper-based Thin Film Microextraction

Zhaoping Xia, Dan Li*, Wei Deng

School of Chemical and Environmental Engineering, Shanghai Institute of Technology, 100 Haiquan Road, Shanghai 201418, P. R. China

** Corresponding author phone/fax: +86-21-60873241; E-mail: dany@sit.edu.cn (D. Li)*

Contents

1. Preparation and Modification of GNRs. GNRs was prepared via sodium borohydride seeding growth protocol [1]. Briefly, seed colloids were prepared by rapidly mixing 9.35 mL of 0.1 M CTAB with 0.25 mL of 0.01 M $HAuCl_4$ in a 100 mL erlenmeyer flask at 30 °C. Next, 0.6 mL of freshly prepared, ice-cold $NaBH_4$ solution (0.01 M) was injected quickly into the mixed solution, followed by continuous stirring for 3 min. The resultant seed solution can be stored at 30 °C for 2 h before use. Then the growth solution was prepared separately by mixing 0.5 mL of $HAuCl_4$ (0.01 M), 0.2 mL HCl (1 M) and 0.1 mL $AgNO_3$ (0.05 M) with 10 mL of CTAB (0.1 M) at room temperature. Finally, 12 μL of gold seeds solution was added slowly into the growth solution at 30 °C. The color of the solution slowly changed from clear to wine red indicated that GNRs (790 nm) were obtained. The resulting GNRs were kept at 5°C before use.

The resultant GNRs were further modified with PATP. Typically, 5 mL of as-prepared GNRs were collected by centrifugation at 8,000 rpm for 10 min to remove excess CTAB, and it was further washed two times by deionized water. The supernatant was removed and the precipitate was further re-dispersed in 5 mL of deionized water. Then 0.5 mL of 1 mM PATP was added into 5 mL of purified GNRs solution. The mixture was incubated at 30 °C for 24 h. Excess PATP in the mixture was removed by centrifugation at 8,000 rpm for 5 min and dispersed in deionized water. The resultant PATP-modified GNRs (GNRs/PATP, 0.8 nM) were kept at 4 °C before use, whose concentrations were estimated by Lambert-Beer Law [2].

2. Preparation of MPA capped CdSe/ZnS QDs. The CdSe/ZnS QDs were prepared in aqueous solution using the method described previously [3]. 100 μL of CdSe/ZnS QDs was dissolved in 2 mL n-hexane. Then 100 μL of MPA and 10 μL of freshly prepared sodium hydroxide (0.1 M) was successive added to QDs solution under mechanical stirring for 30 min. The mixture was purified by centrifugation at 8,000 rpm for 10 min, and the upper solution was removed. Afterward, the precipitates were washed with methanol for 2-3 times. Finally, the resulting QDs/MPA (0.5 μM) was dispersed in deionized water for use.

3. Synthesis of GNRs-QDs@NU-901. GNRs-QDs was obtained by a self-assembly procedure. To a solution of 0.5 μM QDs/MPA in DMF (0.5 mL) was added 0.8 nM GNRs/PATP in DMF (2.0 mL). The mixture was stirred at room temperature ovemight. The concentration of GNRs-QDs was estimated according to the concentration of GNRs by the method reported previously [2]. GNRs-QDs@NU-901 was prepared by the modified Farha's method [4]. Specifically, the Zr-cluster was synthesized at high temperature using a reported procedure [5]. Then, the isolated Zr-cluster powder (36.4 mg) was dispersed in DMF (7 mL) in a 20 mL glass sample vial and glacial acetic acid (4 mL) was added. Next, 2.5 mL of GNRs-QDs dispersion was added and the mixture was vigorously stirred. The H_4TBAPy linker (10 mL, 2 mg/mL in DMF) was injected slowly using a syringe pump (0.05 mL/min) and the reaction was left stirring overnight. To remove excess reagents, the MOFs were washed twice in DMF and solvent exchanged to acetone overnight.

4. Raman Enhancement Factor. The enhancement factor (*EF*) can be calculated using the following formula [6]:

$$EF = (I_{SERS} / I_{bulk}) \times (N_{bulk} / N_{SERS})$$

where I_{SERS} and I_{bulk} are the vibration intensities in the SERS of p-aminothiophenol (PATP) and normal Raman spectra of PATP, respectively. N_{bulk} and N_{SERS} are the number of molecules under laser illumination for the bulk sample, and the number of molecules in the self-assembled monolayers (SAMs), respectively. The N_{SERS} and N_{bulk} values can be calculated on the basis of the estimate of the concentration of surface species or bulk sample and the corresponding sampling areas. It is reported that the average surface density of PATP molecules in densely packed monolayers is approximately one PATP molecule per 0.2 nm^2. Then the surface coverage of PATP monolayer on GNRs-QDs@NU-901 is 8.31×10^{-10} mol cm^{-2} (Γ=1 / [(0.2×10^{-14}) × (6.02×10^{23})] mol cm^{-2}=8.31×10^{-10} mol cm^{-2}). Taking the sampling area (ca. 4 μm in diameter) into account, N_{SERS} has a value of 1.04×10^{-16} mol (N_{SERS} =Γ × π × $(4/2)^2$ μm^2=1.04×10^{-16} mol). For the solid sample, the sampling volume is the product of the area of the laser spot (ca. 10 μm diameter) and the penetration depth (~ 2 μm) of the focused laser beam. Assuming the density of bulk PATP is 1.14 g cm^{-3} (https://www.chemicalbook.com/ProductChemicalPropertiesCB3289884_EN.htm), N_{bulk} can be calculated to be 1.43×10^{-12} mol (N_{bulk}=1.14 g cm^{-3} × π × 25 μm^2 × 2 μm / (125.19 g mol^{-1}) =1.43×10^{-12} mol). For the vibrational mode at 1620 cm^{-1}, the ratio of I_{SERS} to I_{bulk} was about 35.5 (Figure S16), so *EF* was calculated to be 4.88×10^5 (35.5× [1.43×10^{-12}/ (1.04×10^{-16}) = 4.88×10^5).

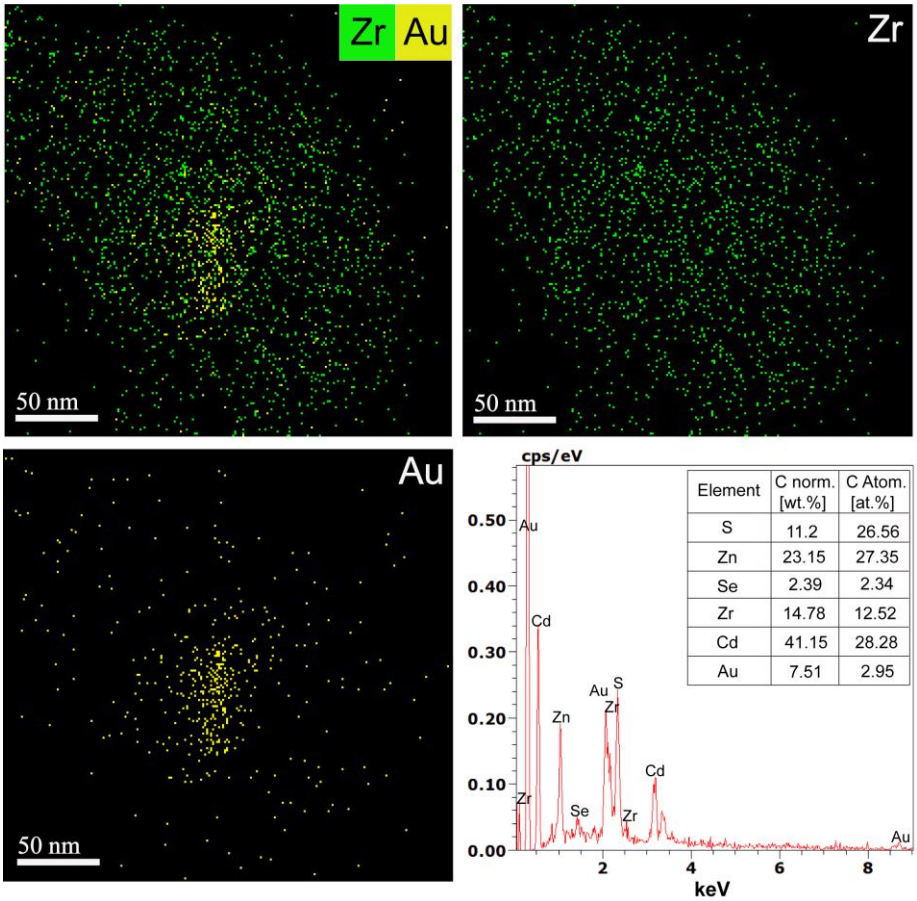

Figure S1. EDX elemental mapping and EDX spectra of GNRs-QDs@NU-901 hybrids.

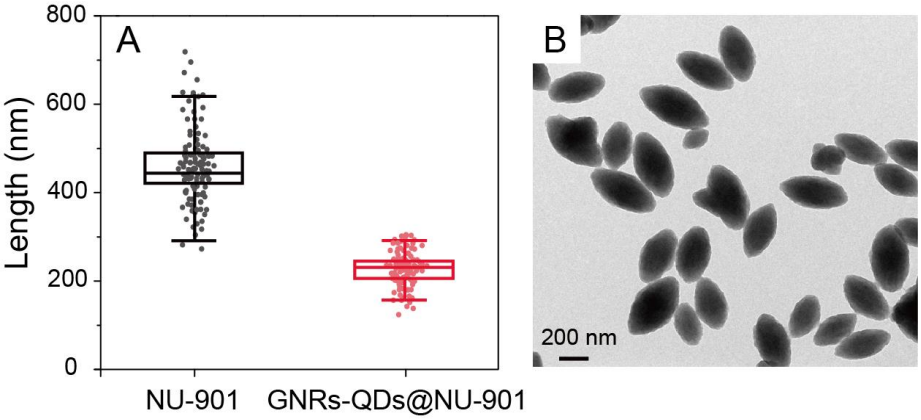

Figure S2. (A) Size-distribution of GNRs-QDs@NU-901 and NU-901 nanoparticles. (B) Representative TEM micrographs of pristine NU-901 crystallites. Length measured along the principal prolate axis.

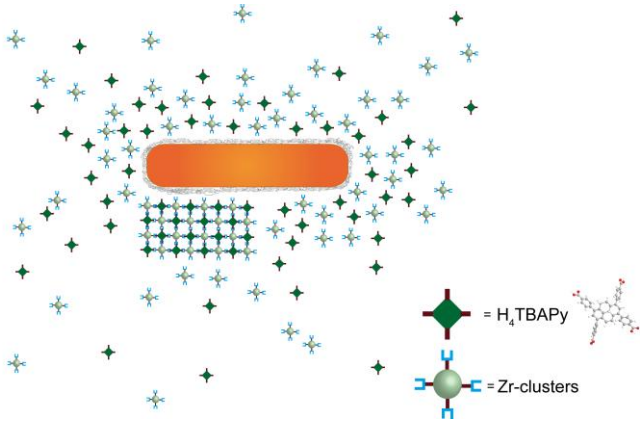

Figure S3. Interactions between PATP and MOF precursors make nucleation more favorable on the GNR.

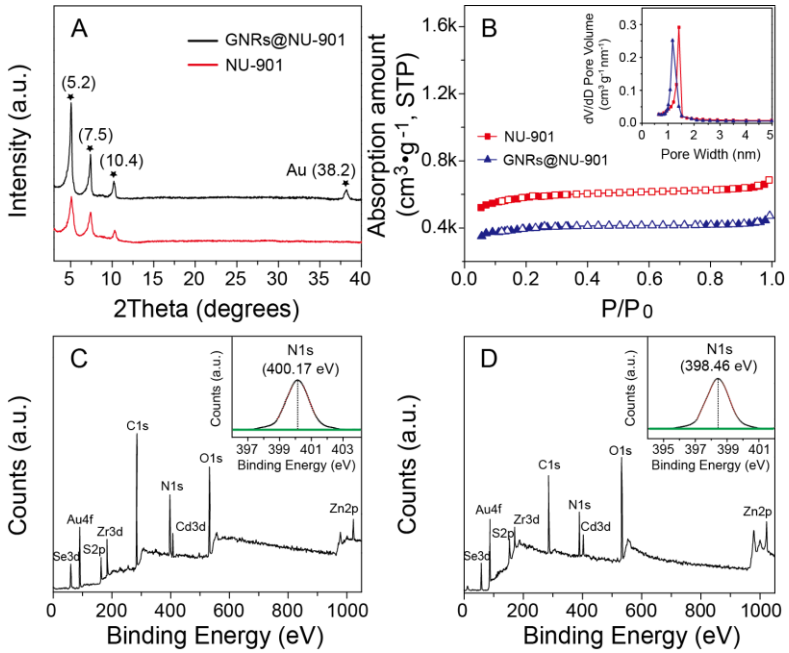

Figure S4. (A) XRD patterns of NU-901 and GNRs@NU-901. (B) N_2 isotherms for pure NU-901 and GNRs@NU-901 at 77 K. The inset is the differential pore size distributions of NU-901 and GNRs@NU-901. XPS spectrum and high-resolution spectrum (insets) of N1s of GNRs-QDs@NU-901 (C) before and (D) after adsorption of BA.

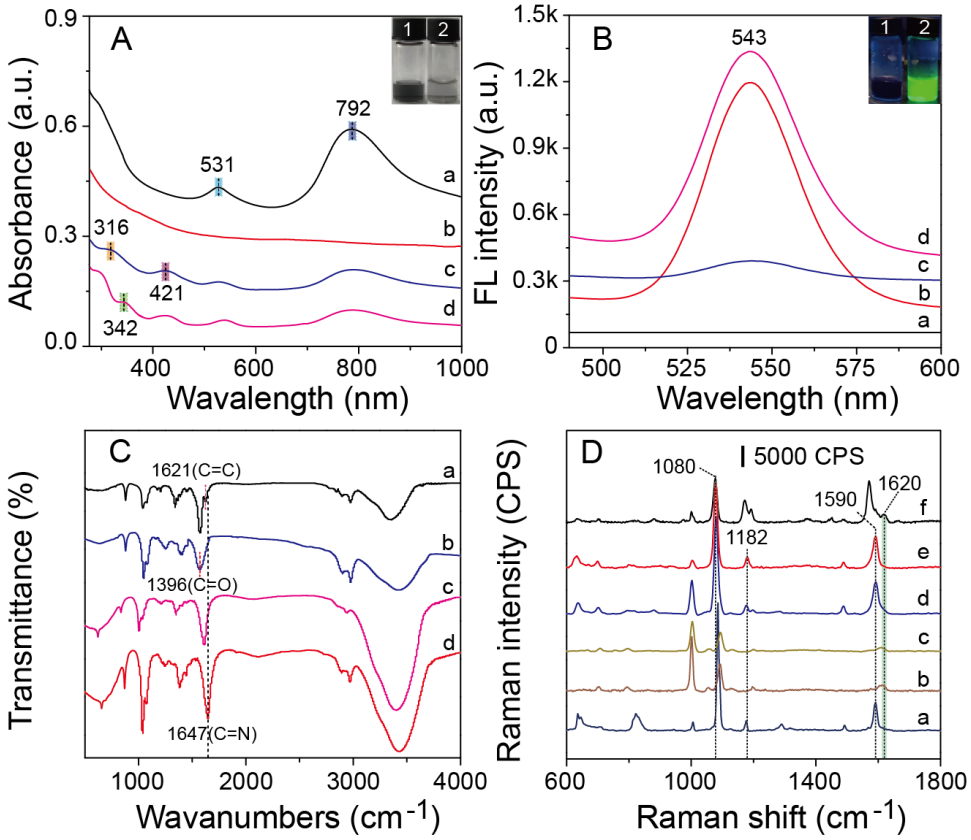

Figure S5. (A) Extinction spectrum and photographs (insets) of (a) GNRs/PATP, (b) QDs/MPA, GNRs-QDs@NU-901 assembly (vial 1, c) before and (vial 2, d) after addition of BA. (B) FL spectrum and photographs (insets, 365-nm excitation) of (a) GNRs/PATP, (b) QDs/MPA, GNRs-QDs@NU-901 assembly (vial 1, c) before and (vial 2, d) after addition of BA. (C) FT-IR spectrum of (a) GNRs/PATP, (b) QDs/MPA, GNRs-QDs@NU-901 (c) without and (d) with the presence of BA. (D) SERS spectrum of (d) GNRs/PATP, GNRs-QDs@NU-901 paper (e) without and (f) with addition of BA. The normal Raman spectra of (a) solid PATP, (b) GNRs@NU-901 and (c) NU-901 served as references.

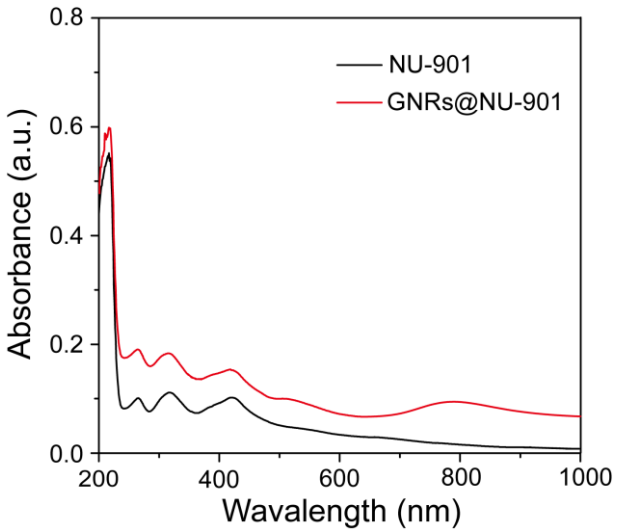

Figure S6. UV-vis spectra of NU-901 and GNRs@NU-901.

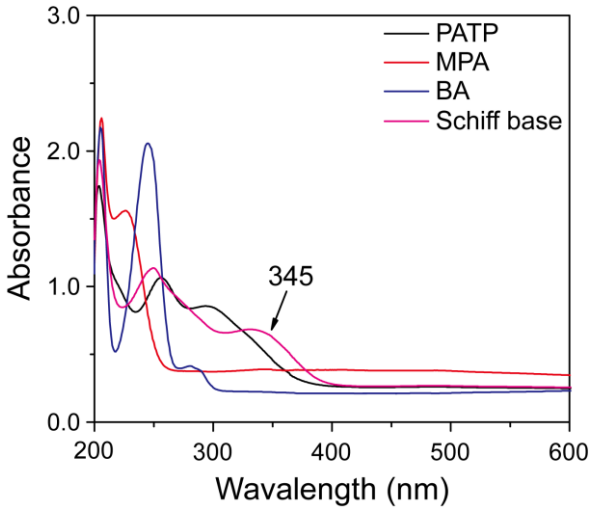

Figure S7. UV-vis absorption spectra of PATP, MPA, BA and Schiff-base complex (PATP-BA).

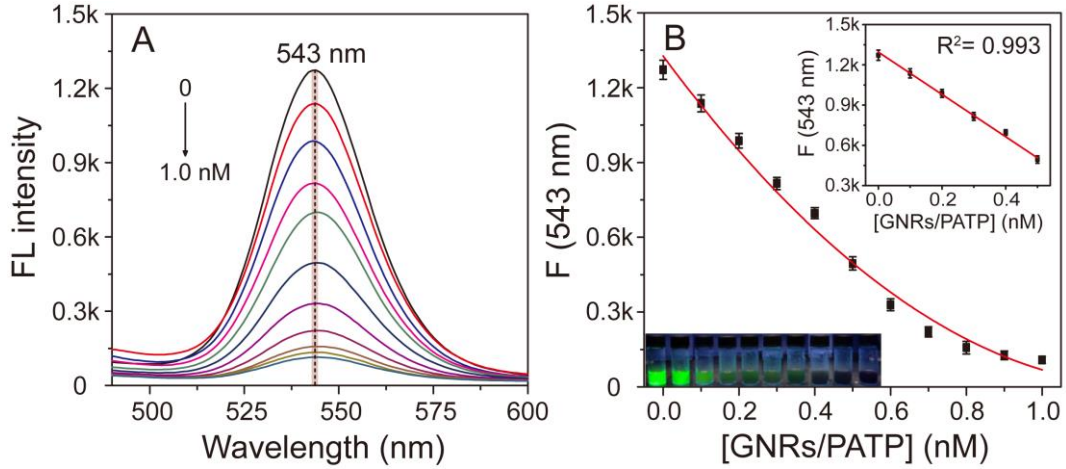

Figure S8. (A) Fluorescence spectra of QDs/MPA with the increase of GNRs/PATP concentrations. (B) Plot of F_{543} versus concentration of GNRs/PATP and photographs (inset, excited by a 365 nm UV lamp) of the QDs/MPA with different concentrations of GNRs/PATP.

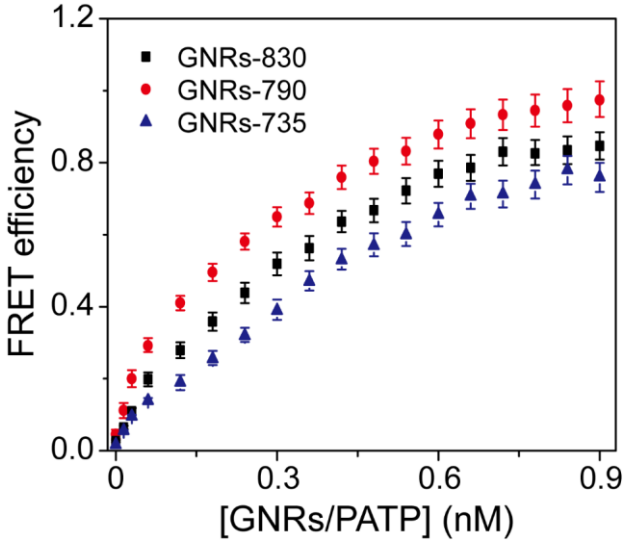

Figure S9. Comparison of FRET efficiencies of GNRs-735, GNRs-790 and GNRs-830. The concentration of the QDs/MPA is 0.5 μM.

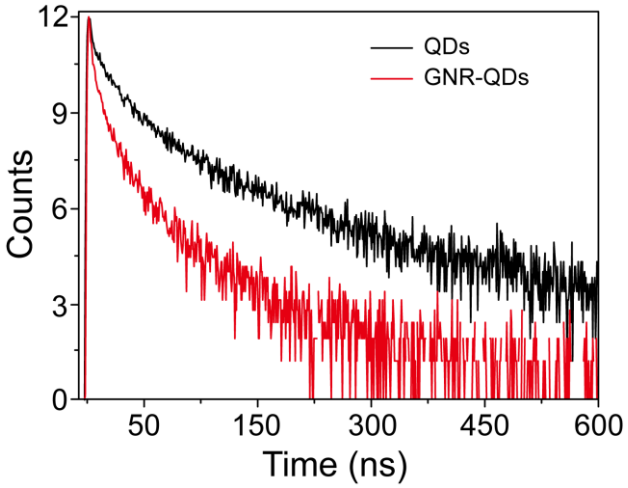

Figure S10. Fluorescence decay curves of CdSe/ZnS QDs and GNR-QDs. The concentrations of GNR and QDs are 10 pM and 5.0 nM, respectively.

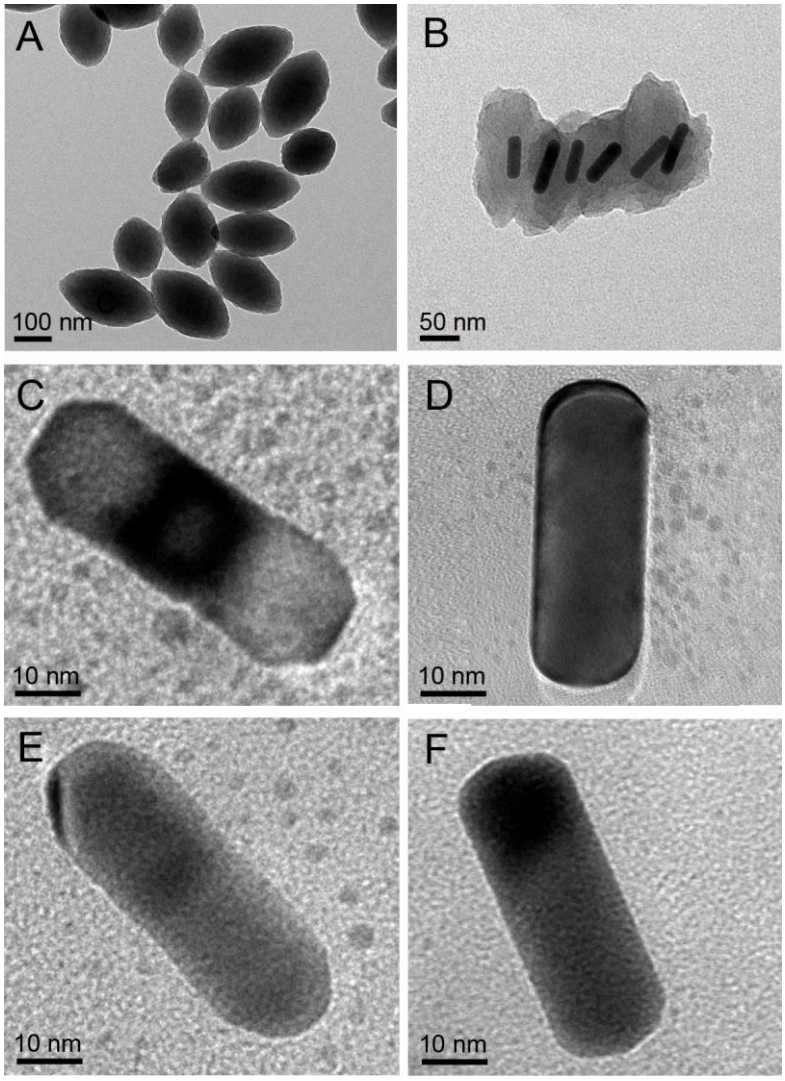

Figure S11. TEM images of (A) NU-901, (B) GNRs@NU-901 and GNRs-QDs@NU-901 with different concentrations (C: 0.01 ppm, D: 0.1 ppm, E: 1 ppm, F: 10 ppm) of BA. The GNRs-QDs@NU-901 is prepared in the presence of 0.8 nM GNRs/PATP and 0.5 μM QDs/MPA (pH 7.0).

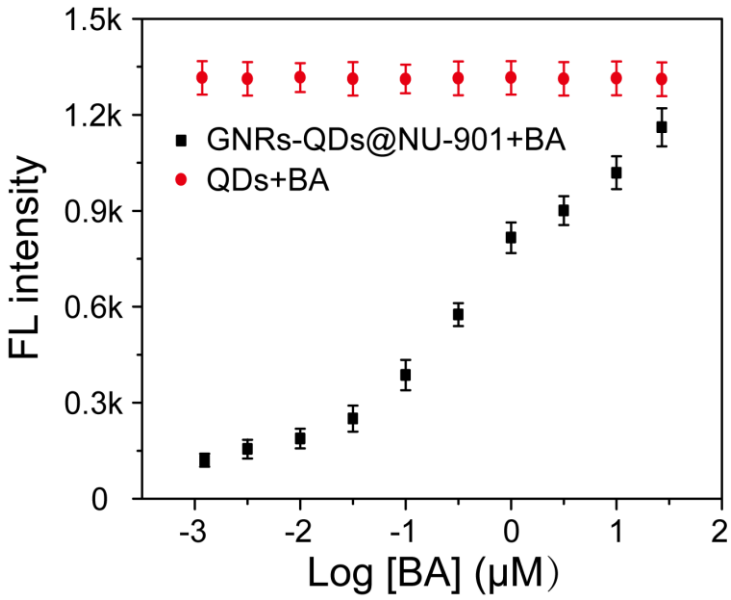

Figure S12. The FL intensity of QDs and GNRs-QDs@NU-901 assemblies in the presence of different BA concentrations.

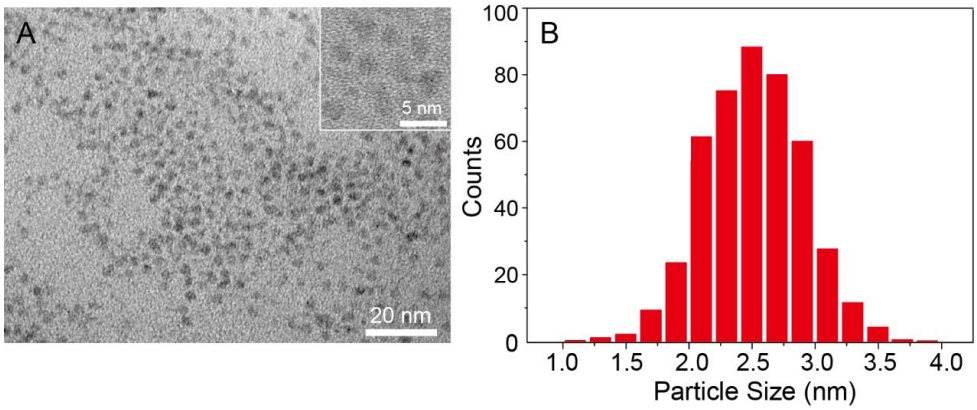

Figure S13. (A) TEM images of the carboxyl-terminated CdSe/ZnS QDs. (B) Histogram of QDs' size distribution from TEM images.

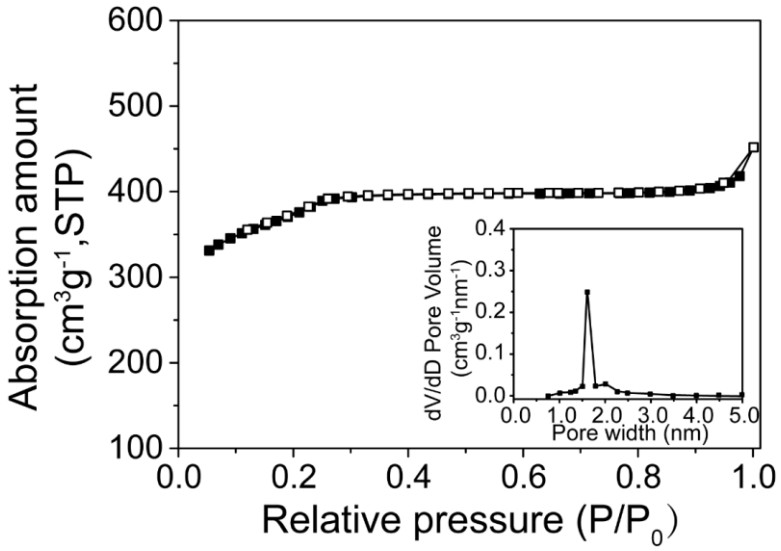

Figure S14. N_2 adsorption isotherms and (inset) pore size distribution of GNRs-QDs@NU-901.

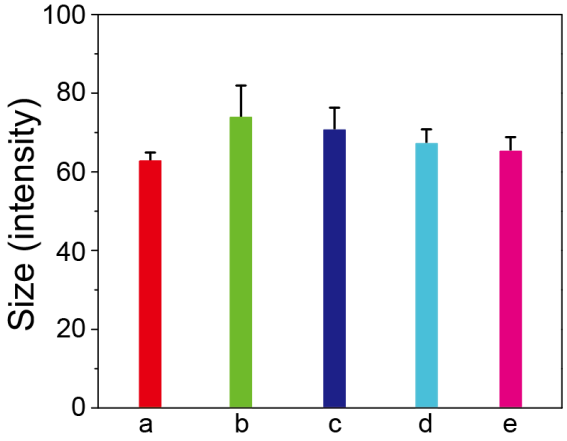

Figure S15. DLS results for studying the interaction of GNR-QDs assemblies with different concentrations of BA (b: 0 ppm, c: 0.1 ppm, d: 1.0 ppm, e: 10 ppm). (a) DLS sizes of GNRs served as reference. The concentrations of GNRs and QDs are 10 pM and 5.0 nM, respectively.

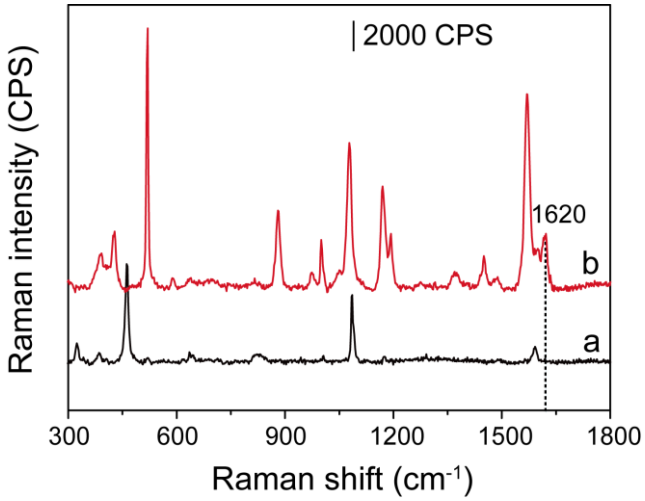

Figure S16. (a) Normal Raman spectrum of solid PATP; (b) SERS spectra of GNRs-QDs@NU-901 paper after adsorption of volatile BA with the concentration of 0.1 ppm, respectively.

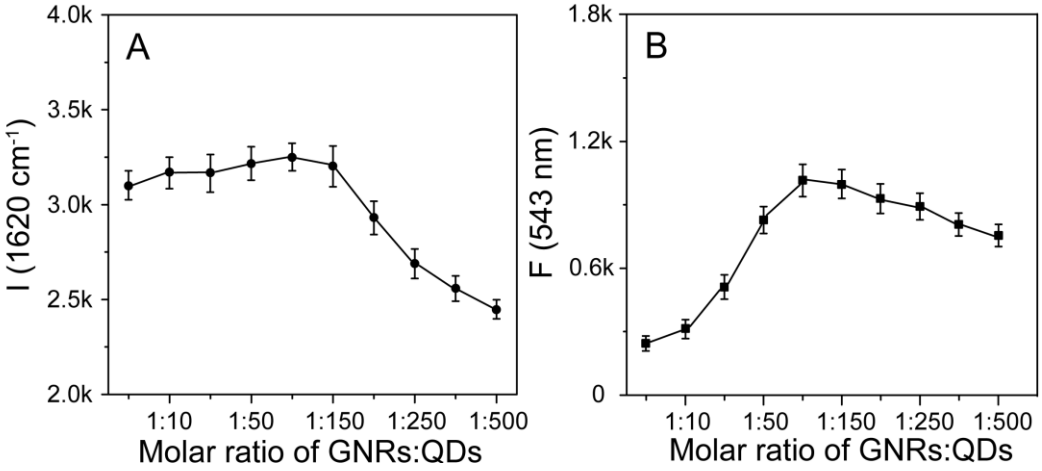

Figure S17. The effects of molar ratio of the GNRs/PATP and the QDs/MPA (GNRs:QDs) on the (A) Raman intensity at 1620 cm^{-1} ($I_{1620cm-1}$) and (B) FL intensity (F_{543} nm) of GNRs-QDs@NU-901 with the presence of BA at 0.1 ppm (pH 7.0). Each data point represents the average value from three measurements on the same samples. Error bars show the standard deviations.

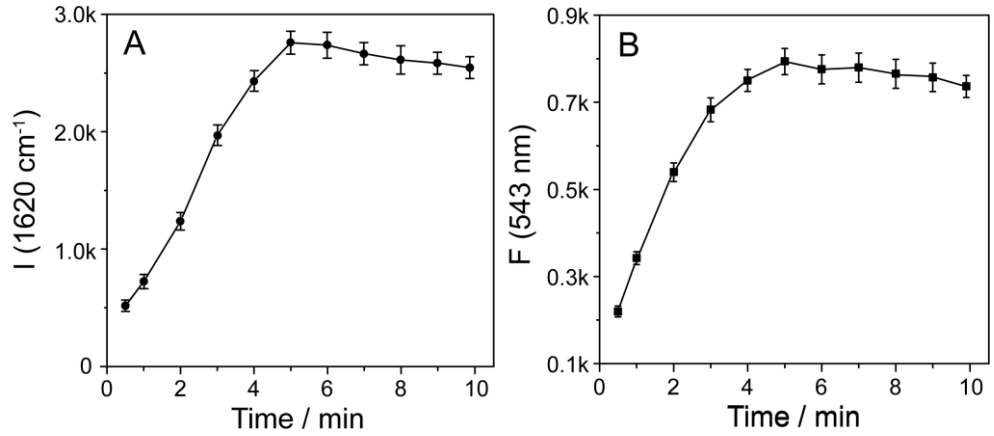

Figure S18. The effects of extraction time on the (A) Raman intensity at 1620 cm^{-1} ($I_{1620cm-1}$) and (B) FL intensity (F_{543nm}) of GNRs-QDs@NU-901 with the presence of BA at 0.1 ppm (pH 7.0). Each data point represents the average value from three measurements on the same samples. Error bars show the standard deviations.

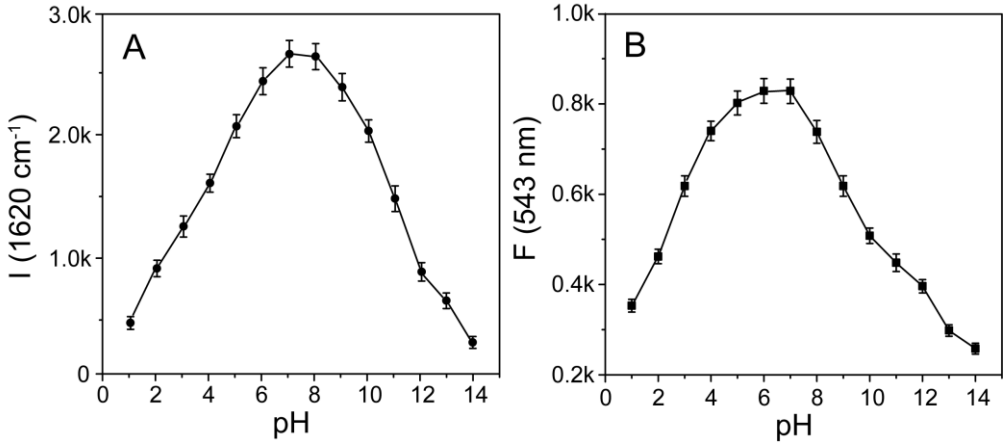

Figure S19. The effects of pH on the (A) Raman intensity at 1620 cm^{-1} ($I_{1620cm-1}$) and (B) FL intensity (F_{543nm}) of GNRs-QDs@NU-901 with the presence of BA at 0.1 ppm. Each data point represents the average value from three measurements on the same samples. Error bars show the standard deviations.

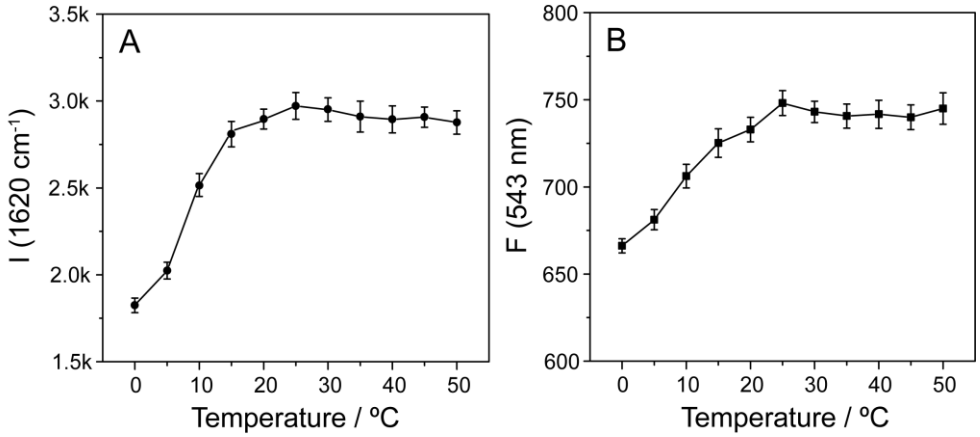

Figure S20. The effects of temperature on the (A) Raman intensity at 1620 cm^{-1} ($I_{1620cm-1}$) and (B) FL intensity (F_{543nm}) of GNRs-QDs@NU-901 with the presence of BA at 0.1 ppm (pH 7.0). Each data point represents the average value from three measurements on the same samples. Error bars show the standard deviations.

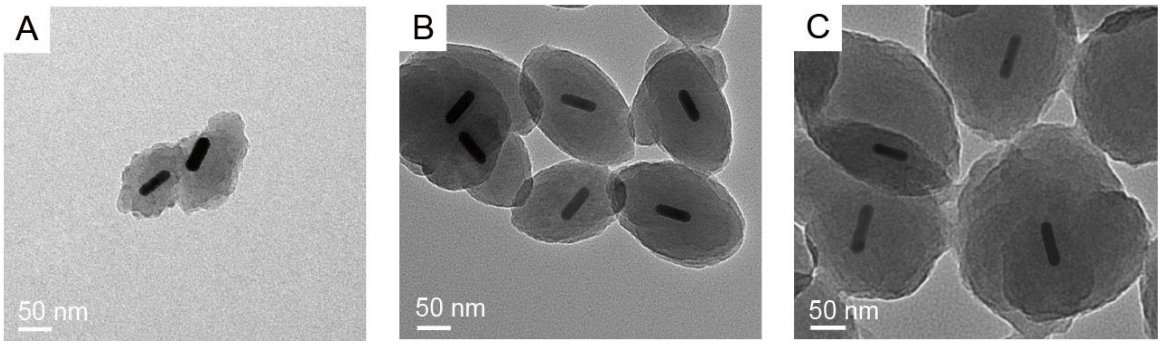

Figure S21. TEM images of NU-901-coated GNRs-QDs with NU-901 thickness (width) of (A) (103±5) nm, (B) (130±10) nm, and (C) (200±12.5) nm, respectively. Thickness (width) measured along the minor axis.

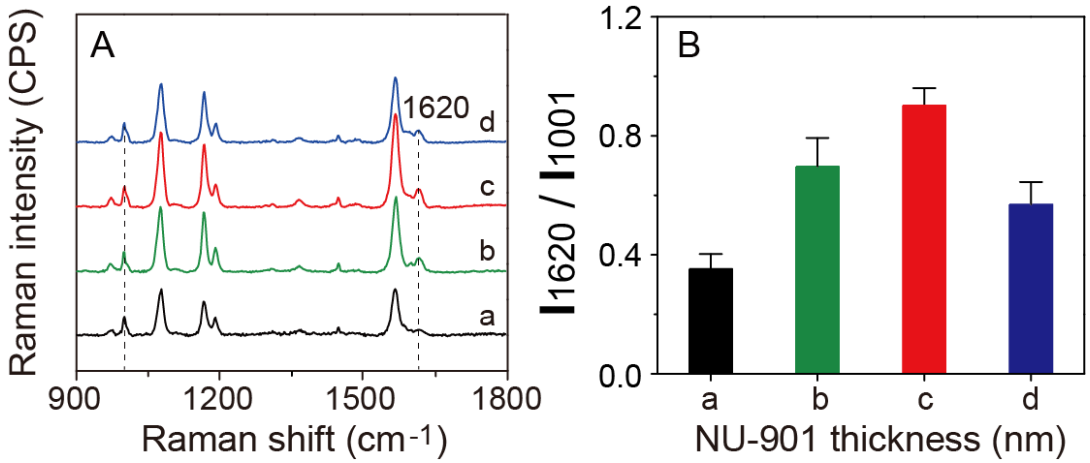

Figure S22. (A) SERS spectra and (B) relative intensity ratio of I_{1620}/I_{1001} of (a) GNRs-QDs and GNRs-QDs@NU-901 with NU-901 shell thickness (width) of (b) (103±5) nm, (c) (130±10) nm, and (d) (200±12.5) nm after the addition of BA (0.1 ppm) at room temperature.

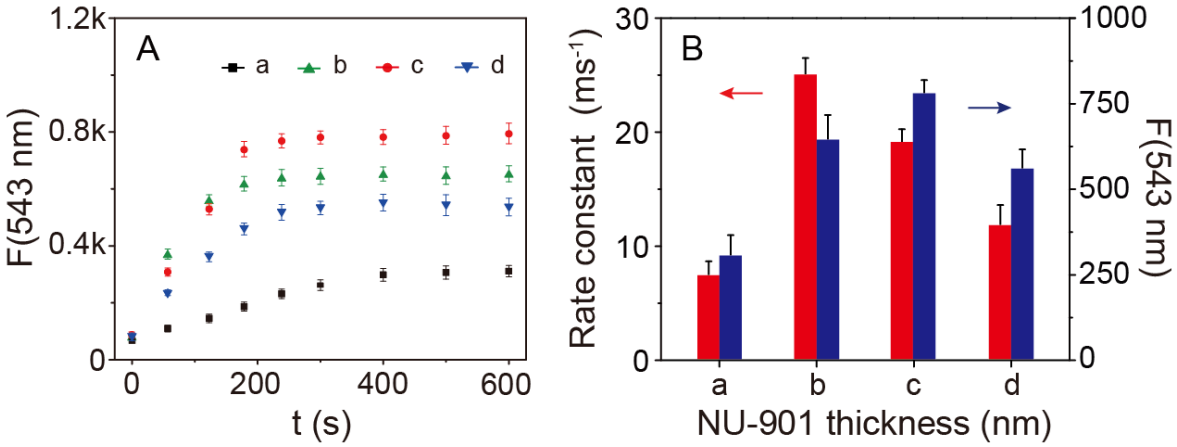

Figure S23. (A) Time-dependent FL of (a) GNRs-QDs and GNRs-QDs@NU-901 with NU-901 shell thickness (width) of (b) (103±5) nm, (c) (130±10) nm, and (d) (200±12.5) nm upon incubation of BA vapor. (B) The effects of NU-901 thickness (width) on the rate constants and FL signals at 543 nm (F_{543nm}) of the respective platforms.

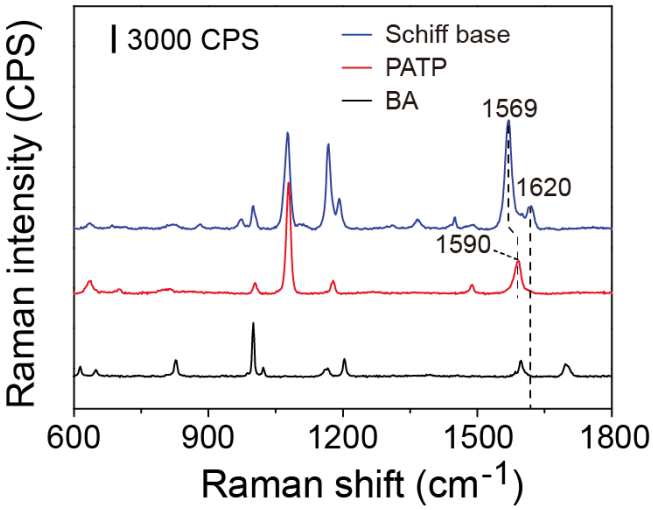

Figure S24. SERS spectra of PATP and Schiff-base complex (PATP-BA). Raman spectra of 1 mM BA served as reference.

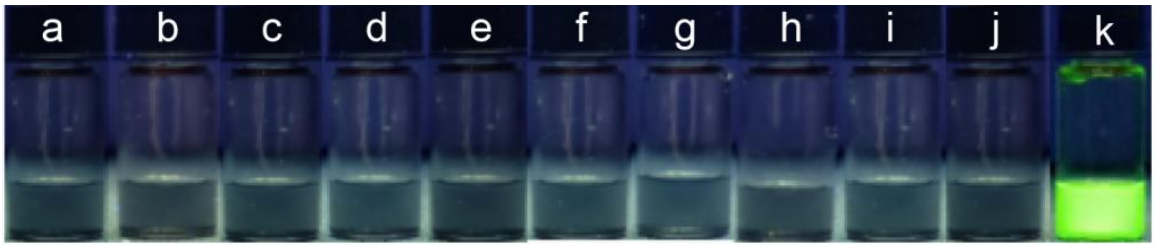

Figure S25. Photographs of the GNRs-QDs@NU-901 with the presence of separate interfering substances (a-j: benzoic acid, acetone, phenol, phenyl alcohol, acetonitrile, formaldehyde, acetaldehyde, ethyl acetate, ethanol, methanol, and k: simultaneous presence of these interfering substances and BA (365-nm excitation).

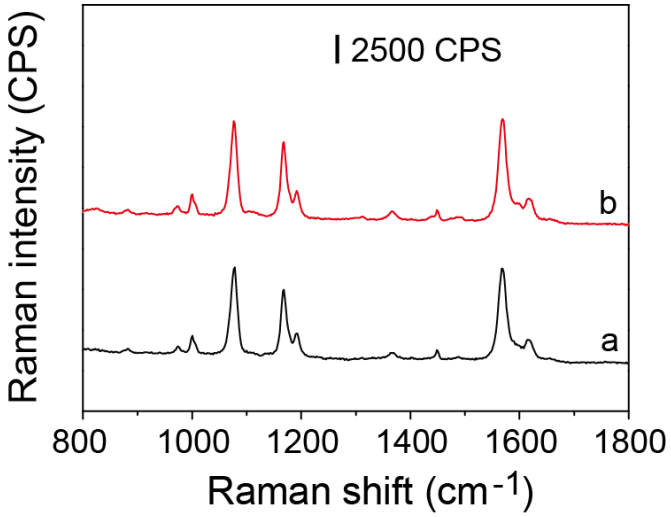

Figure S26. The detection of the BA (10 μL) in the presence of 10 μL potential interfering lung cancer biomarkers (a), including hydrocarbons (n-octane, cyclopentane, isoprene), alcohols (methanol, ethanol), ketones (propanone, cyclohexanon, pentanone), nitriles (acetonitrile), organic acid (benzoic acid), esters (ethyl acetate), aromatic compounds (phenol, phenyl alcohol), H_2S, and NH_3. The upper SERS spectrum (b) was the corresponding GNRs-QDs@NU-901 paper reacted with the gaseous BA.

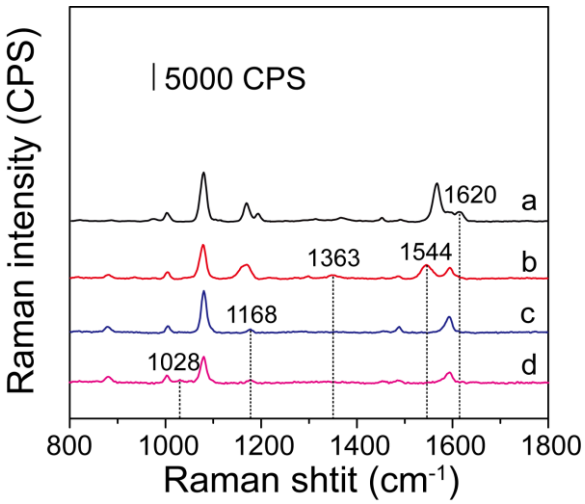

Figure S27. Raman spectra of (a) benzaldehyde ($\nu_{(C=N)}$:1620 cm^{-1}), (b) glyoxal ($\nu_{(C-H)}$:1363 cm^{-1}), (c) glutaraldehyde ($\beta_{(C-C)}$:1168 cm^{-1}) and (d) phenylacetaldehyde ($\nu_{(C-O)}/\beta_{(C-C)}$:1028 cm^{-1}) at the concentration of 10 ppb.

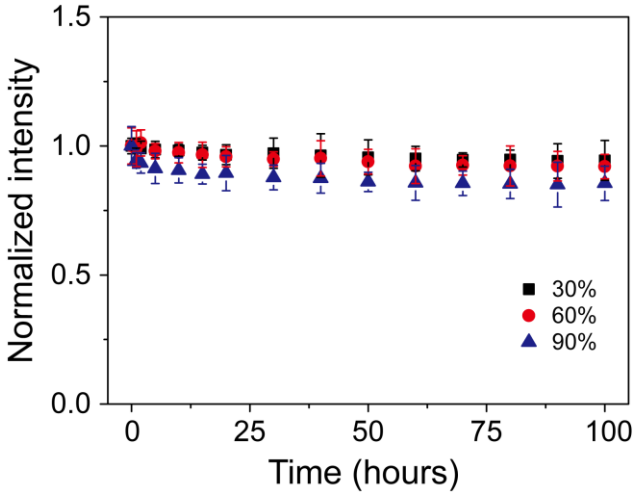

Figure S28. Normalized FL intensity of GNRs-QDs@NU-901-based paper after its exposure to the gaseous BA under different humidity conditions.

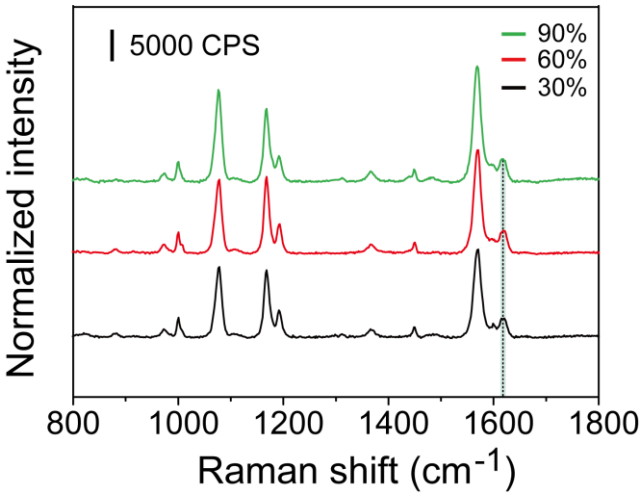

Figure S29. SERS spectra of GNRs-QDs@NU-901-based paper after its exposure to the gaseous BA under different humidity conditions.

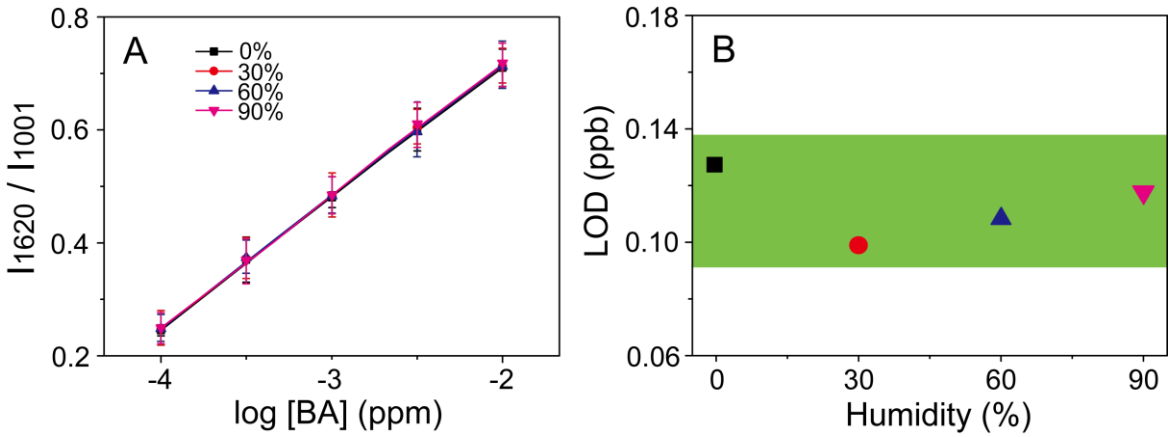

Figure S30. Effect of humidity on SERS performance of GNRs-QDs@NU-901 towards BA. (A) The correlation between the values of I_{1620}/I_{1001} and the BA concentration at different moisture. (B) The LOD of volatile BA at different moisture.

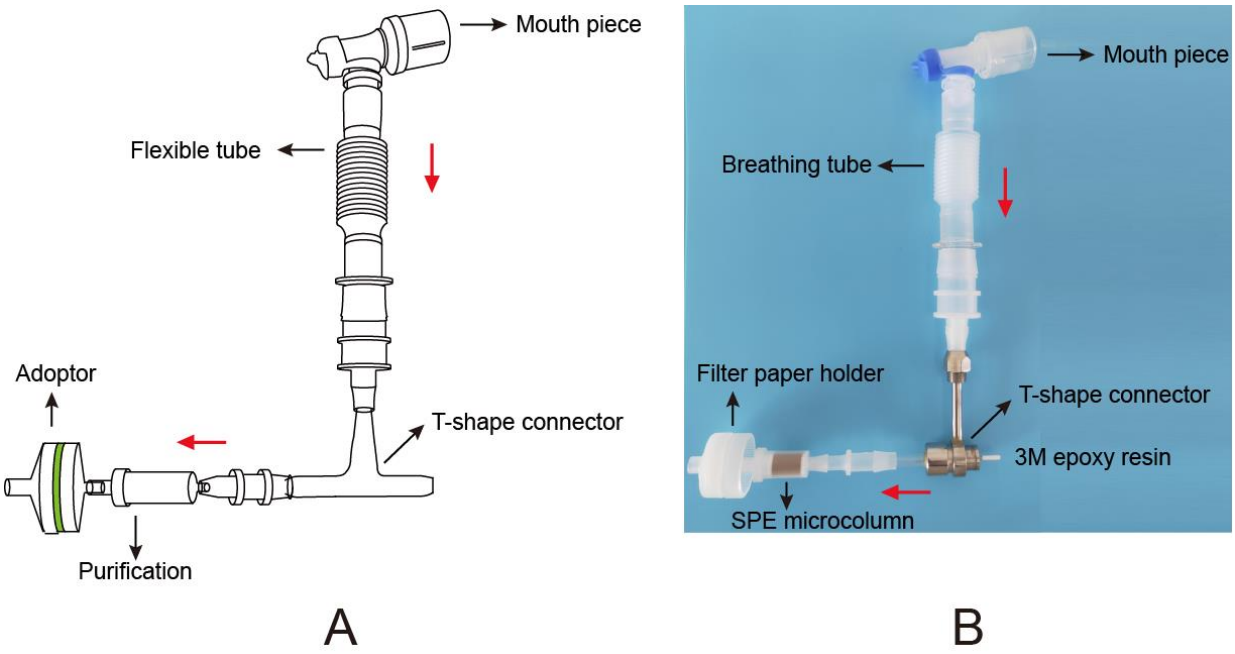

Figure S31. (A) Schematic diagram and (B) photograph of the PTFM device for extraction of volatile BA in human exhalation. The horizontal injection port of nebulizer sealed with 3M epoxy resin. The red arrows indicate the direction of breath samples.

For rapid on-site screening of BA, the participants blow through the mouth piece into PTFM device for a total of 5 min. After PTFM extraction, the fluorescent intensities of GNRs-QDs@NU-901 strips were compared with those of the calibration strips, allowing for qualitative and semi-quantitative assay of BA. SERS spectra were collected from the test strips using the portable Raman spectrometer.

Table S1. Comparing the detection performance of different methods for BA sensing.

Probe	Detection method	Liner range (ppm)	LOD (ppm)	Reference
GSPs@ZIF-8	SERS	1.0×10^{-2}~ 1.0×10^{2}	1.0×10^{-2}	7
Dendritic Ag nanocrystals	SERS	2.0×10^{-3}~ 2.0×10^{2}	1.0×10^{-3}	8
$CuFeS_2$/Au	SERS	1.0×10^{-3} ~ 1.0×10^{2}	1.0×10^{-3}	9
Eu^{3+}@$\{[(CH_3)_2NH_2]_2[Zn_5(TDA)_4(TZ)_4]\cdot4DMF\}_n$	Fluorescence	3.71×10^{-3}~ 2.18×10^{-2}	1.06×10^{-3}	10
carbon nanodots (CDs)	Fluorescence	3.18×10^{-2}~ 7.43×10^{2}	3.18×10^{-2}	11
$\{[Tb(L)(H_2O)((DMF)]\cdot DMF\}_n$	Fluorescence	2.65×10 ~ 2.65×10^{3}	1.19	12
[BMIM][OH]	Electrochemistry	3~ 3×10^{2}	1.7	13
hOBPs	Electrochemistry	1.0×10^{-5}~ 1.0×10^{-2}	1.0×10^{-6}	14
GNRs-QDs@ NU-901	Fluorescence/ SERS	2.0×10^{-3}~ 2.0×10^{3}/ 1.0×10^{-4}~ 1.0×10^{2}	1.2×10^{-3}/ 1.0×10^{-4}	This work

Table S2. Determination of BA in exhaled breath samples and comparison with GC-MS (n=3).

	Samples	Fluorescence (ppb)	SERS (ppb)	GC-MS (ppb)
Lung cancer breath	1	165.4	147.2	158.6
	2	85.44	99.29	95.78
	3	41.59	45.78	39.84
	4	65.82	62.49	55.78
	5	128.6	133.1	137.4
	6	79.05	78.12	63.27
	7	89.72	109.3	94.22
	8	95.61	115.4	109.5
	9	27.31	22.51	33.15
	10	132.1	126.3	122.9
Healthy breath	11	ND	3.283	2.792
	12	ND	1.754	1.087
	13	ND	5.530	4.917
	14	ND	5.724	4.358
	15	ND	3.603	2.947
	16	ND	6.131	7.425
	17	ND	6.173	6.723
	18	ND	3.087	2.216
	19	ND	1.326	0.714
	20	ND	4.955	5.043

ND: lower than LOD

References

(1) Nikoobakht, B.; El-Sayed, M. A. *Chem. Mater.* **2003**, *15* (10), 1957−1962.

(2) Orendorff, C. J.; Murphy, C. J. *J. Phys. Chem. B* **2006**, *110* (9), 3990−3994.

(3) Rogach, A. L.; Franzl, T.; Klar, T. A.; Feldmann, J.; Gaponik, N.; Lesnyak, V.; Shavel, A.; Eychmüller, A.; Rakovich, Y. P.; Donegan, J. F. *J. Phys. Chem. C* **2007**, *111* (40), 14628−14637.

(4) Osterrieth, J. W. M.; Wright, D.; Noh, H.; Kung, C.-W.; Vulpe, D.; Li, A.; Park, J. E.; Van Duyne, R. P.; Moghadam, P. Z.; Baumberg, J. J.; Farha, O. K.; Fairen-Jimenez, D. *J. Am. Chem. Soc.* **2019**, *141* (9), 3893−3900.

(5) Noh, H.; Kung, C.-W.; Islamoglu, T.; Peters, A. W.; Liao, Y.; Li, P.; Garibay, S. J.; Zhang, X.; DeStefano,

M. R.; Hupp, J. T.; Farha, O. K. *Chem. Mater.* **2018**, *30* (7), 2193−2197.
(6) Martín, A.; Pescaglini, A.; Schopf, C.; Scardaci, V.; Coull, R.; Byrne, L.; Iacopino, D. *J. Phys. Chem. C* **2014**, *118* (24), 13260−13267.
(7) Qiao, X.; Su, B.; Liu, C.; Song, Q.; Luo, D.; Mo, G; Wang, T. *Adv. Mater.* **2018**, *30* (5), 1702275.
(8) Zhang, Z.; Yu, W.; Wang, J.; Luo, D.; Qiao, X.; Qin, X.; Wang, T. *Anal. Chem.* **2017**, *89* (3), 1416−1420.
(9) Wen, H.; Wang, H.; Hai, J.; He, S.; Chen, F.; Wang, B. *ACS Sustain. Chem. Eng.* **2019**, *7* (5), 5200−5208.
(10) Zou, J.-Y.; Li, L.; You, S.-Y.; Cui, H.-M.; Liu, Y.-W.; Chen, K.-H.; Chen, Y.-H.; Cui, J.-Z.; Zhang, S.-W. *Dyes Pigments* **2018**, *159*, 429−438.
(11) Li, Y.; Liu, X.; Wu, Q.; Yi, J.; Zhang, G *Sens. Actuators, B* **2018**, *261*, 271−278.
(12) Ding, B.; Cheng, Y.; Wu, J.; Wu, X. M.; Zhang, H. M.; Luo, Y.; Shi, X. F.; Wu, X. X.; Huo, J. Z.; Liu, Y. Y.; Li, Y. *Dyes Pigments* **2017**, *146*, 455−466.
(13) Toniolo, R.; Dossi, N.; Bortolomeazzi, R.; Bonazza, G; Daniele, S. *Talanta* **2019**, *197*, 522−529.
(14) Lu, Y.; Zhang, D.; Zhang, Q.; Huang, Y.; Luo, S.; Yao, Y.; Li, S.; Liu, Q. *Biosens. Bioelectron.* **2016**, *79*, 251−257.